Chinese Chemical Letters 32 (2021) 3916–3920

Contents lists available at ScienceDirect

Chinese Chemical Letters

journal homepage: www.elsevier.com/locate/cclet

Communication

Photoluminescent chiral carbon dots derived from glutamine

Wenyan Ma[a], Bolun Wang[a], Yonggang Yang[b], Jiyang Li[a,*]

[a] State Key Laboratory of Inorganic Synthesis and Preparative Chemistry, College of Chemistry, Jilin University, Changchun 130012, China
[b] Jiangsu Key Laboratory of Advanced Functional Polymer Design and Application Department of Polymer Science and Engineering, College of Chemistry, Chemical Engineering and Materials Science, Soochow University, Suzhou 215123, China

ARTICLE INFO

Article history:
Received 23 February 2021
Revised 10 May 2021
Accepted 13 May 2021
Available online 24 May 2021

Keywords:
Chirality
Carbon dots
Photoluminescence
Circular dichroism
Sensors

ABSTRACT

The integration of luminescence and chirality in carbon dots (CDs) encourages candidates to explore novel functions and applications of CDs, however, the preparation of chiral CDs is very limited. Herein, we report a hydrothermal method to fabricate chiral CDs by utilizing amino acid enantiomers as the precursors. LGln-CDs or DGln-CDs with uniform size of 3–4 nm show excitation-dependent blue fluorescence in solutions. Circular dichroism measurement confirms the opposite optical rotation of chiral CDs in the region from 200 nm to 300 nm, and the signals can be regulated by concentrations of CDs solution. Time-dependent density functional calculation reveals that polypeptides may exist on the surface of CDs due to the polycondensation of L/DGln at high temperature, and the optical activity of CDs originates from the stacking of neighboring carbonyl groups. The facile synthetic methodology proposed will provide potential opportunities for the preparation and application of chiral and chiroptical CDs-based materials.

Carbon dots (CDs), as a class of novel zero-dimensional materials, have aroused much attention since they were first discovered in 2004 [1,2]. Compared with semiconducting quantum dots and organic dyes, CDs have virtues of simple synthesis [3,4], intriguing luminescence [5,6], good biocompatibility, easy functionalization [7,8], *etc*. On account of desirable photophysical properties [9], CDs have presented enormous potential in the fields of analyte detection [10,11], drug convey [12–14], photocatalysis [15,16], light emitting diodes [17–20], bioimaging [21,22], and biosensing [23–26].

Chirality is a phenomenon that an object like a pair of hands cannot coincide with its mirror image. Most biomolecules including peptides, sugars, proteins, amino acids and others are identified as mirror symmetric [27]. They may exhibit opposite effects in the same crucial biological reaction [28]. In recent years, some artificial nanostructures with handedness, such as chiral metal nanoparticles [29–31], chiral photonic bioderived films [32,33], chiral carbon nanodots [34], chiral plasmonic nanostructure [35], had been explored. Among them, chiral CDs with excellent optical activity have aroused wide interest of researchers in the fields of biology and chemistry.

Usually, glucose [36], amino acids [37] and amines as the smallest chiral parts of life could be employed to synthesize chiral CDs with superior symmetrical signals by using hydrothermal method [37], microwave [34], pyrolysis [38] and electrolysis [39]. However, the variety of CDs with chirality is still rare and CDs precursors are limited [39–41]. Moreover, there remains unclear on the mechanism of chiral CDs, which includes their formation process, possible chirality and chiral reconstruction, and tunable radiative relaxation [42]. Revealing the mechanism and regulations on structures and properties of chiral CDs would certainly be a huge boost for their applications.

In this work, we present a mild hydrothermal method to fabricate chiral CDs derived from glutamine (named L- or D-Gln) and citric acid (CA) (Fig. 1). The morphology of chiral CDs was investigated by transmission electron microscopy (TEM) characterization. As shown in Fig. 2a, as-synthesized LGln-CDs are spherical nanoparticles with size of 3.5 ± 1.0 nm (Fig. S1 in Supporting information). The high-resolution TEM image demonstrates the distinct lattice spacing of 0.18 nm, corresponding to the [102] plane of graphitic carbon (the inset of Fig. 2a) [43]. TEM and HRTEM images of DGln-CDs also show a similar morphology and diameter of 3–4 nm (Figs. S2a and S3 in Supporting information). Fourier transform infrared (FTIR) spectra were carried out to study the functional groups on chiral CDs. As shown in Fig. 2b, the broad bands at 3344 cm^{-1}, 3125 cm^{-1} and 3011 cm^{-1} are corresponding to the stretching vibration of O–H, N–H and =C–H bonds, respectively. The strong bands at 1403 cm^{-1} and 1227 cm^{-1} are the stretching and bending vibrations of C–N and C–O=C groups [44]. The peak located at 1622 cm^{-1} is primarily governed by amide bonds,

* Corresponding author.
E-mail address: lijiyang@jlu.edu.cn (J. Li).

https://doi.org/10.1016/j.cclet.2021.05.021
1001-8417/

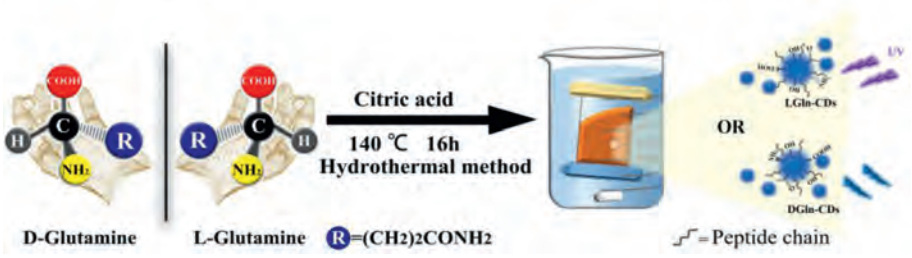

Fig. 1. Synthetic strategy of LGln-CDs or DGln-CDs *via* hydrothermal method.

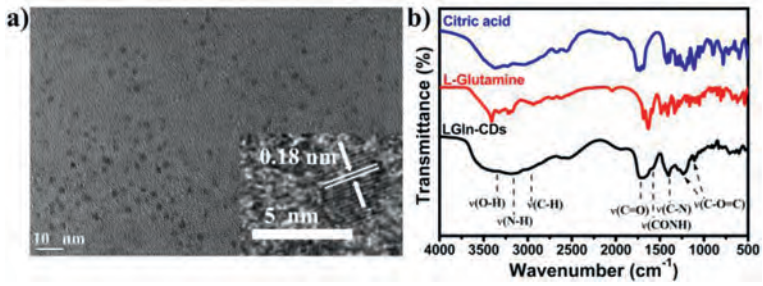

Fig. 2. (a) TEM image of LGln-CDs (Inset: the corresponding HRTEM image of individual LGln-CDs). (b) FT-IR spectrum of citric acid (blue line), L-Glutamine (red line) and LGln-CDs (black line).

suggesting the parallel stacking of peptide chains [45], and C=O groups can be observed at 1715–1735 cm^{-1} [46]. The results of FTIR analysis indicate the existence of oxygen and nitrogen functional groups, particular peptide chains on the surface of LGln-CDs, similar with that of DGln-CDs (Fig. S2b in Supporting information). It is noted that bands from L/DGln-CDs become wider and fewer compared to those precursors, which confirms the polymerization of raw materials during the hydrothermal process [37,47].

X-ray photoelectron spectroscopy (XPS) further reveals the chemical states of the functional groups on L/DGln-CDs surface. The full scan spectrum of LGln-CDs in Fig. S4a (Supporting information) illustrates that C, N, O are the main elements of prepared chiral CDs. The C 1s XPS spectrum of LGln-CDs (Fig. S4b in Supporting information) could be fitted into four peaks at ~284.60 eV, ~285.75 eV, ~286.90 eV, and ~288.67 eV, corresponding to the C=C/C–C, C–N/C–O, C=N and –COOH, respectively [48]. N 1s spectrum (Fig. S4c in Supporting information) shows three different chemical states, including C–N=C (399.86 eV), N-$(C)_3$ (400.40 eV) and N–H (401.62 eV). For O 1s (Fig. S4d in Supporting information), the peak at 531.85 eV attributes to the C=O, the peak at 532.94 eV originates from C–OH/C–O–C, and the one at 533.67 eV belongs to C–O [49]. As shown in Fig. S5 (Supporting information), DGln-CDs also exhibit the similar chemical element states as LGln-CDs. The XPS results of chiral CDs are consistent with those of FTIR spectra.

The luminescence properties of L/DGln-CDs are studied. The fluorescence spectra of L/DGln-CDs are displayed in Fig. 3a and Fig. S6a (Supporting information). L/DGln-CDs exhibit bright blue fluorescence under UV lamp (λ = 365 nm). Optimal excitation and maximum emissions of L/DGln-CDs are 360 nm and 450 nm, respectively. They also show excitation-dependent emissions as shown in Fig. 3b and Fig. S6b (Supporting information). The fluorescence emission of CDs shows red-shifting from 433 nm to 478 nm when excited from 300 nm to 400 nm. Besides, the fluorescence intensity of LGln-CDs increases with the extension of hydrothermal reaction time (Fig. S7 in Supporting information), which suggests the gradual formation of CDs cores during the hydrothermal synthesis. In details, some sub-fluorophores with very weak photoluminescence are generated at the early stage. Over time, with the crosslinking or aggregation, these sub-fluorophores can be immobilized and their vibration and rotation are partly restricted, which leads to the enhancement of emission intensity [50]. When pH value increases from 5 to 10, the fluorescence intensity of L/DGln-CDs shows significant enhancement (Fig. S8 in Supporting information). The UV–vis absorption spectra of L/DGln-CDs show a characteristic absorption peak in the region of 210−250 nm that can be extended to the visible spectrum (Fig. 3a and Fig. S6a), which is originating from the aromatic π-π^* transition of C=C bonds [51]. In addition, another typical band located at 340 nm is the transition of unbonded lone pair of electrons to the π^* orbital, which is arising from the N=H, C=O bonds on the surface of CDs [52]. Based on the above results, it can be found that LGln-CDs and DGln-CDs have very similar photoluminescence properties. It is hard to observe the evident distinction about fluorescence and UV–vis absorption between LGln-CDs and DGln-CDs. This could be attributed to the same chemical structure of similar precursors.

Although L/DGln-CDs display same types of transition in UV–vis wavelength region, they have extremely different ellipticity. As illustrated in Fig. 3c, these two kinds of CDs display opposite behavior for left or right polarized light, and their circular dichroism signals are located at 217 nm and 232 nm. As shown in Fig. S9 (Supporting information), the anisotropy factors (g factor) of chiral CDs are calculated to be 1.0 × 10^{-4} and 2.39 × 10^{-3}, respectively. The circular dichroism spectra of L/DGln-CDs exhibit extreme symmetry about X coordinate axis. Compared with L-Gln and D-Gln in Fig. 3d, signal of L/DGln-CDs at 217 nm can be attributed to the inheritance of chiral precursor structure and additional signal at 232 nm could be a novel asymmetric structure. Thus, the hydrothermal synthesis of chiral CDs proposed in this work not only maintains the chiral center of L/D-Gln well, but also produces a new chiral structure center on the surface of CDs. Such new chiral center of CDs is necessary to be further studied.

As comparison with UV–vis absorption peaks at 217 nm and 340 nm, it is clear that chiral CDs show no circular dichroism signal around 340 nm, while a signal around 232 nm is observed. To further understand the origin of such circular dichroism signal, quantum chemistry calculations have been applied to simulate the circular dichroism spectra, which is a good way to ex-

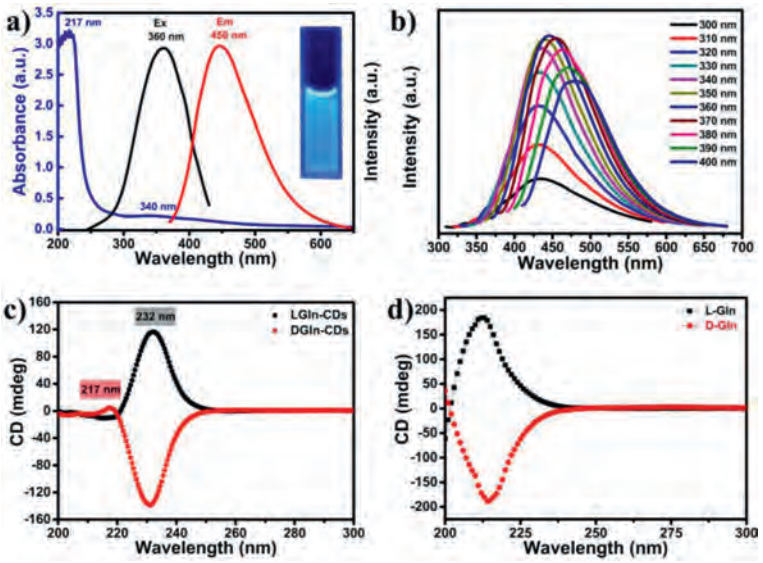

Fig. 3. (a) The absorption curve (blue line), fluorescence excitation (black line) and emission spectra (red line) of LGln-CDs, Inset: the photo of LGln-CDs excited at 365 nm UV light. (b) Excitation-dependent behavior of LGln-CDs when excited from 300 nm to 400 nm. (c) Circular dichroism spectra of LGln-CDs and DGln-CDs solutions with concentration of 2.0 mg/mL. (d) Circular dichroism spectra of L-Gln and D-Gln.

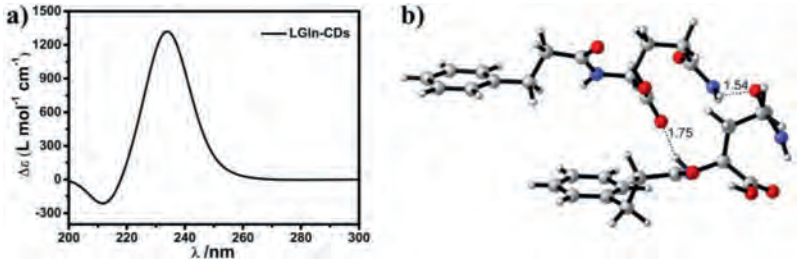

Fig. 4. (a) Simulated ECD spectra of LGln-CDs at the level of TD-B3LYP/6-31G+(d,p). (b) The geometry-optimized structures of LGln-CDs at the B3LYP/6-31G+(d,p) level.

plain the source of chirality of LGln- or DGln-CDs. The circular dichroism signals of chiral CDs are identified at the wavelength lower than 250 nm. Thus, they should originate from the stacking of neighboring carbonyl groups on the surface of CDs. During the hydrothermal process, L- or D-Gln should undergo polycondensation and carbonization sequentially at high temperature. L- or D-Gln and citric acid should incipiently undergo polycondensation and polypeptide chains may be generated, followed by crosslinking of the chains caused by molecular interactions. With the increasing carbonization degree, CDs consist of carbon cores inside and polypeptides outside as functional groups were obtained. Due to carbonization, it will inevitably lead to a racemization within the carbon cores. Therefore, no circular dichroism signals are identified at longer wavelength (above 250 nm), indicating that there is no chiral stacking of the aromatic rings or the induction of the surrounding chiral environment (Fig. 4a).

Take LGln-CDs as an example, the calculations of the electrostatic circular dichroism (ECD) spectra of a simulated LGln-CDs structure are carried out using the TD-B3LYP/6–31G+(d,p) level with Gaussian 09 quantum package [53] . The achiral carbon nanoparticle is instead by two phenyl groups. The polypeptides on the surface of CDs are instead by two neighbouring L-Gln residues. Electronic excitation energies (nm) and rotational strengths ($\Delta\varepsilon$) were calculated for LGln-CDs. In order to cover the 200–300 nm range, 30 transitions were calculated. The simulated spectra are in good agreement with the experimental spectral data, and the L-Gln configuration could be reliably assigned to the simulated LGln-CDs in Fig. 4b.

Moreover, the asymmetric stability of LGln- and DGln-CDs has been studied. CDs are dissolved into Britton-Robinson buffer solution with different pH values. The circular dichroism position of LGln-CDs blue-shifts slightly by 2 nm as the pH value increases from 5.0 to 10.0, and the ellipticity of LGln-CDs gradually increases with the increase of environmental alkalinity (Fig. S10a in Supporting information). DGln-CDs also show similar tendency (Fig. S11a in Supporting information), which means that acids and alkalis have little effect on circular dichroism of as-made CDs. Temperature stability of chiral CDs is also investigated. As shown in Fig. S10b (Supporting information) and S11b, when heating from 65 °C to 100 °C, there is no noticeable change in peak location and ellipticity of LGln-CDs and DGln-CDs, showing excellent temperature stability. In addition, circular dichroism signal remains unchanged in NaCl solutions with different ionic strength (Figs. S11c and d in Supporting information). The above results demonstrate that L/DGln-CDs prepared in this work have excellent chiroptical stability in the strong alkalinity and acidity, high temperature, and high ionic strength.

Interestingly, the circular dichroism location is related to the concentrations of chiral CDs solution. As shown in Fig. 5a, the signals have blue-shifted to 209 nm when concentration of LGln-CDs decreased from 2.0 mg/mL to 6.75×10^{-2} mg/mL. Whereas, continuing decrease the concentration on this basis, the position of the signal remains unchanged. To further illustrate the relationship between concentration and circular dichroism signal, we perform TEM characterization at concentrations of 2.0 mg/mL and 6.75×10^{-2} mg/mL. As shown in Figs. 5c and d, it can be seen that

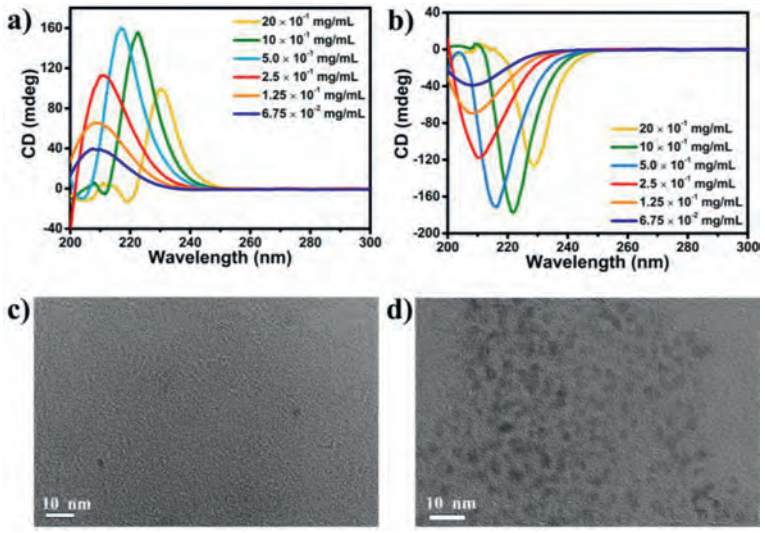

Fig. 5. Circular dichroism spectra of (a) LGln-CDs and (b) DGln-CDs aqueous solutions with various concentrations. TEM photograph of LGln-CDs solution with concentration of (c) 6.75×10^{-2} mg/mL and (d) 20×10^{-1} mg/mL.

LGln-CDs display different morphology with monomer dispersion and aggregation. Therefore, we assume that the shift of dichroism signals is caused by aggregate states of LGln-CDs in high concentration [54]. At the isolated state, the intermolecular H-bonds between neighboring peptides are not formed. Therefore, the CDs signal may originate from the electron transition within the carbonyl groups. With the increasing concentration of CDs, the aggregates are formed through the intermolecular H-bonds between neighboring peptides. At this time, the CDs signal may originate from the electron transition between neighboring carbonyl groups, leading to the red shifting of circular dichroism signals. DGln-CDs also have the same relationships with its concentration (Fig. 5b).

It is worth noting that the synthesis method presented here is not only suitable for glutamine enantiomers, but also for other amino acid enantiomers to synthesize chiral CDs with good optical properties. As shown in Fig. S12 (Supporting information), chiral CDs have been synthesized from the enantiomers of histidine and arginine as chiral raw materials. These two chiral CDs have opposite circular dichroism in the ultraviolet region. L/DArg-CDs show good mirror symmetry at 230 nm and 259 nm, and L/DHis-CDs have a mirror symmetry peak at 250 nm. These chiral CDs all exhibit blue fluorescence and excitation-dependent emission behaviors. These results prove the universality of this synthetic method, which may provide the possibility to enrich the types of chiral CDs and opens up the future of CDs.

The as-prepared L/DGln-CDs show fluorescence quenching to Fe^{3+}. Responses of LGln-CDs to 12 common metal ions are investigated (Fig. S13a in Supporting information, F and F_0 is the FL intensity of LGln-CDs in the presence and absence of metal ions). Fig. S13b shows that fluorescence intensity of LGln-CDs is strongly quenched (over 80%) by Fe^{3+}compared with other metal ions (such as Al^{3+}, Co^{2+}, Zn^{2+}, Ni^{+}, Cu^{2+}, Mn^{2+}, K^{+}, Na^{+}, Ca^{2+}, Cd^{2+}, Cs^{2+}). When added from 10 to 80 μmol/L, PL intensity gradually decreases, which can be fitted by equation of $F_0/F = 0.003[Fe^{3+}]$ (mmol/L) + 0.977 ($R^2 = 0.998$, $K_{sv} = 3.5 \times 10^3$) with minimum detection limit (DL) of 0.014 mmol/L. Due to its sensitivity, selectivity and luminescence stability, as-made CDs can be used as a fluorescent probe in practice. Different lake water samples are also collected for testing. The concentration of Fe^{3+} is 0.01 mol/L for each sample (Fig. S13d in Supporting information) and they have slight fluctuation in the degree of FL quenching. As shown in Fig. S14 (Supporting information), DGln-CDs also have similar fluorescence detection ability for Fe^{3+} ions with DL of 0.011 mmol/L and K_{sv} of 3.2×10^3. It is known that Fe^{3+} can be coordinated with abundant functional groups on the surface of CDs [55]. The electrons of CDs would transfer to the Fe^{3+}, forming hole/non-radiative electron recombination, which leads to the fluorescence quenching [56]. The fluorescence lifetimes of L/DGln-CDs decreases when Fe^{3+} added (Figs. S15 and S16 in Supporting information), which further indicates the coordination between CDs and Fe^{3+} ions.

In this work, a facile and universal hydrothermal method has been demonstrated to synthesize series of novel chiral CDs with opposite optical rotation using amino acid enantiomers as precursors. The as-prepared LGln- or DGln-CDs possess similar particle size and excitation-dependent photoluminescence properties. According to the theoretical calculation results, the chirality of LGln- or DGln-CDs originates from surface groups while not carbon core, which is due to the stacking of neighboring carbonyl groups of peptides on the CDs. The concentrations of CDs solution may affect the dispersion and aggregation of CDs, which leads to the electron transitions occurring within the carbonyl groups at low concentration and between neighboring carbonyl groups at high concentration, thus further regulating the circular dichroism signals. More in-depth insight of formation mechanism of chiral CDs and further applications of such chiral CDs are undergoing.

Declaration of competing interest

The authors declare no conflict of financial interest.

Acknowledgments

This work was financially supported by the National Natural Science Foundation of China (No. 21621001) and the 111 Project (No. B17020).

Supplementary materials

Supplementary material associated with this article can be found, in the online version, at doi:10.1016/j.cclet.2021.05.021.

References

[1] X.Y. Xu, R. Ray, Y.L. Gu, et al., J. Am. Chem. Soc. 126 (2004) 12736–12737.
[2] F. Li, D.Y. Yang, H.P. Xu, Chem. Eur J. 25 (2019) 1165–1176.
[3] W.D. Li, Y. Liu, B.Y. Wang, et al., Chin. Chem. Lett. 30 (2019) 2323–2327.
[4] B.Y. Wang, J.K. Yu, L. Sui, et al., Adv. Sci. (2020) 2001453.
[5] L. Xiao, H.D. Sun, Nanoscale Horiz. 3 (2018) 565–597.
[6] J.J. Du, N. Xu, J.L. Fan, W. Sun, X.J. Peng, Small 15 (2019) 1805087.
[7] B.L. Wang, Y. Mu, H.Y. Zhang, et al., ACS Cent. Sci. 5 (2019) 349–356.
[8] B.L. Wang, Y. Yu, H.Y. Zhang, et al., Angew. Chem. Int. Ed. 58 (2019) 18443–18448.
[9] H.Q. Song, Y.H. Li, L. Shang, et al., Nano Energy 72 (2020) 104730.
[10] Y.F. Wang, B.L. Wang, H.Z. Shi, et al., Inorg. Chem. Front. 5 (2018) 2739–2745.
[11] Y.F. Wang, X.S. Liu, M.K. Wang, et al., Sens. Actuators B 329 (2021) 129115.
[12] J. Tang, B. Kong, H. Wu, et al., Adv. Mater. 25 (2013) 6569–6574.
[13] W.Q. Li, Z.G. Wang, S.J. Hao, et al., Nanoscale 10 (2018) 3744–3752.
[14] H. Wang, C.Q. Liu, Z. Liu, J.S. Ren, X.G. Qu, Small 14 (2018) 1703710.
[15] Y.Z. Han, H. Huang, H.C. Zhang, et al., ACS Catal. 4 (2014) 781–787.
[16] W.D. Li, Y.X. Zhao, Y. Liu, et al., Angew. Chem. Int. Ed. 60 (2021) 3290–3298.
[17] Y.L. Zhang, Q. Ran, Q. Wang, et al., Adv. Mater. 31 (2019) 1902368.
[18] J.L. Wang, F. Zhang, Y.L. Wang, Y.Z. Yang, X.G. Liu, Carbon 126 (2018) 426–436.
[19] F.L. Yuan, Z.B. Wang, X.H. Li, et al., Adv. Mater. 29 (2017) 1604436.
[20] C. Sun, Y. Zhang, K. Sun, et al., Nanoscale 7 (2015) 12045–12050.
[21] G.E. LeCroy, S.T. Yang, F. Yang, et al., Coord. Chem. Rev. 320–321 (2016) 66–81.
[22] K. Hola, Y. Zhang, Y. Wang, et al., Nano Today 9 (2014) 590–603.
[23] S. Chung, R.A. Revia, M.Q. Zhang, Adv. Mater. (2019) doi:10.1002adma.201904362.
[24] Z.L. Peng, X. Han, S.H. Li, et al., Coord. Chem. Rev. 343 (2017) 256–277.
[25] J. Zhang, S.H. Yu, Mater. Today 19 (2016) 382–393.
[26] S.J. Zhu, Q.N. Meng, L. Wang, et al., Angew. Chem. Int. Ed. 125 (2013) 4045–4049.
[27] C.L. Hao, L.G. Xu, H. Kuang, C.L. Xu, Adv. Mater. 32 (2019) 1802075.
[28] J. Crassous, Chem. Soc. Rev. 38 (2009) 830–845.
[29] T.G. Schaaff, G. Knight, M.N. Shafigullin, R.F. Borkman, R.L. Whetten, J. Phys. Chem. B 102 (1998) 10643–10646.
[30] C. Gautier, T. Bürgi, ChemPhysChem 10 (2009) 483–492.
[31] J. Kumar, K.G. Thomas, L.M. Liz-Marzan, Chem. Commun. 52 (2016) 12555–12569.
[32] V. Cherpak, V.F. Korolovych, R. Geryak, et al., Nano Lett. 18 (2018) 6770–6777.
[33] H.Z. Zheng, W.R. Li, W. Li, et al., Adv. Mater. 30 (2018) 1705948.
[34] L. Đorđević, F. Arcudi, A. D'Urso, et al., Nat. Commun. 9 (2018) 3442.
[35] A. Querejeta-Fernández, G. Chauve, M. Methot, J. Bouchard, E. Kumacheva, J. Am. Chem. Soc. 136 (2014) 4788–4793.
[36] M.L. Zhang, H.B. Wang, B. Wang, et al., Small 15 (2019) 1901512.
[37] L.L. Hu, Y. Sun, Y.J. Zhou, et al., Inorg. Chem. Front. 4 (2017) 946–953.
[38] R. Malishev, E. Arad, S.K. Bhunia, et al., Chem. Commun. 54 (2018) 7762–7765.
[39] L.L. Hu, H. Li, C.A. Liu, et al., Nanoscale 10 (2018) 2333–2340.
[40] Y.L. Zhang, L.L. Hu, Y. Sun, et al., RSC Adv. 6 (2016) 59956–59960.
[41] T.N. Pham-Truong, T. Petenzi, C. Ranjan, H. Randriamahazaka, J. Ghilane, Carbon 130 (2018) 544–552.
[42] Y. Ru, L. Ai, T.T. Jia, et al., Nano Today 34 (2020) 100953.
[43] S. Sahu, B. Behera, T.K. Maiti, S. Mohapatra, Chem. Commun. 48 (2012) 8835–8837.
[44] X.X. Shi, Y.L. Hu, H.M. Meng, et al., Sens. Actuators B 306 (2020) 127582.
[45] X. Geng, Y.Q. Sun, Z.H. Li, et al., Small 15 (2019) 1901517.
[46] M.L. Zhang, L.L. Hu, H.B. Wang, et al., Nanoscale 10 (2018) 12734–12742.
[47] Y.Y. Wei, L. Chen, J.L. Wang, et al., RSC Adv. 9 (2019) 3208–3214.
[48] H. Ding, S.B. Yu, J.S. Wei, H.M. Xiong, ACS Nano 10 (2016) 484–491.
[49] X.R. Liu, S.X. Zhang, H. Xu, et al., ACS Appl. Mater. Interfaces 12 (2020) 47245–47255.
[50] S.J. Zhu, Y.B. Song, J.R. Shao, X.H. Zhao, B. Yang, Angew. Chem. Int. Ed. 54 (2015) 14626–14637.
[51] B.L. Wang, Y. Mu, C.H. Zhang, J.Y. Li, Sens. Actuators B 253 (2017) 911–917.
[52] Z. Guo, Z.Q. Zhang, W. Zhang, et al., ACS Appl. Mater. Interfaces 6 (2014) 20700–20708.
[53] M.J. Frisch, G.W. Trucks, H.B. Schlegel, et al., Gaussian (2013) 09 Revision D.01 Gaussian.
[54] L.L. Zhou, D.X. Zheng, B. Wu, Y.Q. Zhu, L.L. Zhu, ACS Appl. Nano Mater. 3 (2020) 946–952.
[55] K.G. Qu, J.S. Wang, J.S. Ren, X.G. Qu, Chem. Eur. J. 19 (2013) 7243–7249.
[56] Y. Song, C.Z. Zhu, J.H. Song, et al., ACS Appl. Mater. Interfaces 9 (2017) 7399–7405.